Fluorescence Lifetime Probe of Biomolecular Conformations

Xiangguo Shi and Joel H. Parks
Rowland Institute at Harvard, Cambridge, Massachusetts, USA

Methods have been developed to measure the fluorescence lifetime versus temperature of trapped biomolecular ions derivatized with a fluorescent dye. Previous measurements for different sequences of polyproline peptides demonstrated that quenching rates are related to conformations and their spatial fluctuations. This paper presents the results of extending these methods to study the conformational dynamics of larger biomolecules. Vancomycin–peptide noncovalent complexes in the 1+ charge state were studied as a function of temperature for different W-KAA peptide chiralities (L-LDD, D-LDD, L-DLL). Fluorescence-quenching rates, k_q, were found to be stereoselective for these different chiralities with relative magnitudes k_q(L-LDD) > k_q(D-LDD) > k_q(L-DLL). The variation in fluorescent quenching resulting from switching the chirality of the single Trp residue was readily detectable. Molecular dynamics analysis of complexes formed by W-KAA (L-LDD) and W-KAA(L-DLL) indicates that increased flexibility in the (L-DLL) complex is correlated with reduced quenching rates. Fluorescence measurements were also performed for the Trp-cage protein comparing quenching rates in the 1+, 2+, and 3+ charge states for which $k_q^{+} \gg k_q^{2+} \approx k_q^{3+}$. Measurements of a sequence including a single-point mutation infer the presence of a salt-bridge structure in the 1+ charge state and its absence in both the 2+ and 3+ states. Molecular dynamics structures of Trp-cage indicate that a salt bridge in the 1+ charge state produces more compact conformations leading to larger quenching rates based on the quenching mechanism. In both these experimental studies the fluorescence-quenching rates were consistent with changes in structure induced by either intermolecular or intramolecular interactions. (J Am Soc Mass Spectrom 2010, 21, 707–718) © 2010 American Society for Mass Spectrometry

Previous measurements [1] of the lifetime of a fluorescent dye covalently bound to polypeptide ions exhibited a quenching rate that depends both on the separation of the dye to a Trp side chain and on the strength of electrostatic fields in the vicinity of the dye. Quenching rates were found to depend on specific peptide sequences giving rise to different conformations and spatial fluctuations characterized by each conformation. Consequently, lifetime measurements provide an opportunity to extract information sensitive to local molecular arrangements and, perhaps more importantly, changes in that arrangement determined by intramolecular and intermolecular interactions.

This paper applies lifetime measurements to study two larger biomolecules: the vancomycin–peptide noncovalent complex and the Trp-cage protein. The structures of these biomolecules have been identified in NMR solution measurements; and each has been studied previously in gas-phase measurements. Results of gas-phase studies of the vancomycin–peptide complex infer that specific changes in the peptide ligand chirality lead to different hydrogen binding networks and thus to different conformations. Gas-phase measurements and calculations of Trp-cage protein indicate that the presence of a salt bridge structure and the resulting conformations depend on the protein charge state. Consequently, these biomolecules present an opportunity to measure the extent that fluorescence-quenching rates characterize conformations associated with changes in intermolecular and intramolecular interactions.

This paper includes a brief review of the fluorescence-quenching results in polyproline peptides [1], which displays the form of the quenching rate temperature dependence and discusses a quenching mechanism suggested by that data. Following sections present measurements of the quenching rates for stereoisomers of the vancomycin–peptide complex and charge states of the Trp-cage protein. Trends of the experimental quenching rates will be compared with preliminary analyses of molecular dynamics simulations. It will be shown that changes in the calculated structures are consistent with measured trends in these quenching rates.

Experimental

Vancomycin–Peptide Materials

The peptides listed in Table 1 were synthesized by BioMer Technology (Concord, CA) and purified by reversed-phase HPLC to a stated purity of >70% before

Address reprint requests to Dr. J. H. Parks, The Rowland Institute at Harvard, 100 Edwin H. Land Blvd., Cambridge, MA 02142, USA. E-mail: parks@rowland.harvard.edu

1044-0305/10/$32.00
doi:10.1016/j.jasms.2010.01.009

Published online January 25, 2010
Received November 17, 2009
Revised January 13, 2010
Accepted January 13, 2010

shipment. Vancomycin hydrochloride was purchased from MP Biomedicals Inc. (Solon, OH). The BODIPY dye analogue of rhodamine-6G BODIPY-R6G was obtained from Invitrogen (Eugene, OR). The chemical structure and excitation and emission spectra of BODIPY-R6G have been published elsewhere [2]. The fluorescent dye was coupled to the primary amine of vancosamine without a linker and separated from the reaction solution by HPLC (HP1100; Hewlett-Packard, Palo Alto, CA) in our laboratory. Acetonitrile (>99.9%) and distilled, deionized water were obtained from Fisher Scientific (Fair Lawn, NJ) and VWR (West Chester, PA), respectively.

Dye-derivatized vancomycin (VD) and VD–peptide complexes were prepared in 20% acetonitrile/80% water with 5 mM ammonium acetate (pH 4.5). In these solutions the concentration of VD was typically 15 μM, whereas the concentrations of peptides were varied from 15 to 60 μM, and optimized to obtain a sufficient number of trapped ions for fluorescence lifetime measurements. A schematic of the noncovalent complex formed between VD and the tetrapeptide W-KAA (L-LDD) based on solution NMR structures of vancomycin and KAA (LDD) [3] is shown below indicating the dye binding position on vancomycin, the Trp position on the KAA peptide.

Trp-Cage Materials

Derivatized peptides were synthesized by BioMer Technology (Hayward, CA, USA) and purified by reversed-phase HPLC to a stated purity of >70% before shipment. The BODIPY analogue of tetramethylrhodamine BODIPY-TMR was obtained from Invitrogen (Eugene, OR, USA). Two peptide amino acid sequences were synthesized NLYIQWLKDGGPSSGRPPPSK-(BODIPY-TMR)-$CONH_2$ and NLYIQWLKNGGPSSGRPPPSK-(BODIPY-TMR)-$CONH_2$. The first sequence is the same as that of Trp-cage [4] with the addition of lysine at the C-terminus to allow for conjugation of the dye via the ε-amine. The second sequence is the D9N variant which replaces the aspartic acid residue at position 9 by asparagine. Attachment of the dyes does not significantly alter the emission or excitation spectra (data not shown). Ammonium acetate (>98%) was obtained from Sigma (St. Louis, MO), and acetonitrile (>99.9%), ammonium bicarbonate (>99%), and distilled, deionized water were obtained from Fisher Scientific (Fair Lawn, NJ), Mallinckrodt (Hazelwood, MO), and VWR (West Chester, PA), respectively. Electrospray solutions contain 10 μM analyte in aqueous or 1:1 acetonitrile/water solutions. Ammonium bicarbonate and acetate (10 mM) are added for pH stabilization.

Ion Trap Mass Spectrometry

Experimental procedures are similar to those described previously [1, 5]. In brief, all experiments were performed in a quadrupole ion trap mass spectrometer built in-house. Ions under investigation were transferred to the gas-phase by a homebuilt nanoESI through borosilicate glass needles prepared by a micropipette puller (model P-87; Sutter Instruments, Novato, CA). The solutions were electrosprayed at a potential of 0.8 ~ 1.0 kV and the flow rate were 60 ~ 200 nL/min. Ions enter the first differentially pumped chamber of the instrument through a heated stainless steel capillary (length = 4.2 cm, i.d. = 0.5 mm). The ion-source parameters were optimized to be "soft" enough that noncovalent complexes could survive during desolvation. Ions were loaded into the trap through ion lenses and a 23 cm octopole ion guide. The ions of interest were mass-selected by ejecting the unwanted low mass range ions using ramped RF voltages and high mass range ions by resonant frequency excitation. The trap temperature could be varied from 150 K to 560 K by heating or cooling the copper trap housing (model 965 temperature controller; Watlow, St. Louis, MO) with a temperature precision of ±1 °C. The He background gas was also heated to the trap temperature and the He pressure in the trap was $\sim 3 \times 10^{-5}$ Torr and pulsed to $\sim 2 \times 10^{-3}$ Torr to thermalize ions with mass < 500 u at the He temperature before laser excitation. Equilibrating ions having a mass > 500 u was dominated by interactions with the background black body thermal radiation. After the fluorescence lifetime measurement, ions were ejected into a Channeltron electron multiplier (model 7596; K and M Electronics Inc., West Springfield, MA) to record the mass spectra. The ESI-MS instrument was mass calibrated over an appropriate range for each biomolecular species.

Fluorescence Lifetime Measurement

The lifetime measurement instrumentation [1] excites trapped ions of interest with a solid-state Nd:YVO_4 laser (Vanguard 2000-HM532; Spectra-Physics, Irvine, CA) at 532 nm and average power of 10 mW. The pulse width was 12 ps (FWHM) and the repetition rate was reduced from 80 to 26.7 MHz through pulse picking by a transverse field modulator (Conoptics, Danbury, CT). Multi-pulse data cycles were repeated until sufficient photons were collected for the fluorescence lifetime analysis. The exposure time of ions to laser excitation was varied from 100 ms to 800 ms depending on temperature to optimize S/N without inducing ion fragmentation. At the end of each data cycle, trapped ions were ejected into the Channeltron detector.

The laser beam path was oriented orthogonal to the ion source beam and the detection path. Emitted fluorescence was collected through an optimized lens/filter optical configuration and detected by a gallium arsenide photomultiplier (H7421-40; Hamamatsu Photonics, Hamamatsu, Japan) having an instrument response of ~0.5 ns. A histogram-accumulating real-time processor (TimeHarp 200; PicoQuant, Berlin, Germany) was used for time-correlated single photon counting. The resulting fluorescence decay curves were deconvo-

luted and fit by a stretched exponential model implemented in the FluoFit data analysis package (ver. 4.0, PicoQuant). All fluorescence lifetime measurements were replicated three times for each data point.

Molecular Dynamics Simulations

Vancomycin–Peptide Complexes

Molecular modeling was performed on an SGI Onyx 3200 workstation running Insight II/Discover (97.0; Accelrys Software Inc., San Diego, CA). The original structure of vancomycin obtained from the protein data bank [6] was used as the reference. Structures of singly protonated dye-vancomycin ($[VD + H]^+$, and dye-vancomycin–peptide complexes with each of the peptides shown in Table 1 were built using the Biopolymer builder of Insight II. In all cases, the protonation site was positioned on the secondary amine as discussed below. Initial cation structures of dye derivatized vancomycin (VD) and vancomycin–peptide (VD-WKAA) complexes were energy minimized using the CFF91 force field [7]. Conformational space of complex ions was explored using molecular dynamics (MD) simulations performed at 150 to 500 K in 50 K intervals in vacuum with a 1.0 fs time step. Simulated annealing (SA) [8] was used to generate multiple starting structures for simulations. For SA, the molecule is initially energy minimized and cooled from 500 to 0 K over a period of 1 ns. A starting structure resulting from SA is then minimized and followed by a 1 ns MD simulation during which structures are sampled at 0.1 ps intervals.

Trp-Cage

The molecular dynamics simulations of Trp-cage are described in detail elsewhere [9] and are reviewed here briefly. Simulations are performed using the GROMACS software package [10, 11] with the OPLS/AA force field [12]. The conformation determined by NMR [4] is used as the initial structure. To match the molecule used for experiments, an amidated lysine residue was attached to the C-terminus, and the BODIPY-TMR dye was attached to the side-chain amine of Lys21. Force field parameters for the dye were taken as much as possible from analogues (similar chemical groups) available in the OPLS/AA force field. Charge locations for the sequences calculated by these simulations and presented in this paper are discussed in detail below. Replica exchange MD (REMD) simulations [13] of 500 ns were performed at 16 different temperatures, namely at 280, 284, 289, 295, 302, 310, 319, 329, 340, 352, 365, 379, 394, 410, 427, and 445 K, respectively. Both the 2+ and the 3+ ions were simulated with an integration time step of 2 fs for 10 ns during which structures are sampled at 0.1 ps intervals.

Results and Discussion

Polyproline Peptides

Recent fluorescence lifetime studies [1] of polyproline peptides as a function of temperature demonstrated that the quenching interaction between a covalently attached fluorescent dye and a tryptophan residue yields information about the conformation and conformational fluctuations of the peptide. Experiments were performed on small peptides to eliminate the additional dynamics associated with protein unfolding. Amino acid sequences of up to 12 residues were designed to vary the separation between the dye and tryptophan and also between the dye and a single protonation site by including spacers of relatively rigid polyproline chains [14] of different lengths. Polyproline ions having sequences dye-$[Pro]_n$-Arg^+-Trp were studied to determine the dependence of the dye lifetime on the separation of the dye and tryptophan residue. Peptide sequences dye-Trp-$[Pro]_n$-Arg^+ were also studied to investigate the role of electrostatic interactions between the charge and the dye Trp pair in the quenching process. In these sequences, the important side-chain fluctuations are limited to tryptophan, arginine, as well as the dye, which helps interpretation of the data and comparison with molecular dynamics simulations. The primary results of these measurements will be reviewed here and the reader is referred to reference [1] for details.

Fluorescence Quenching Rates for Dye-$[Pro]_n$-Arg^+-Trp

Fluorescence-quenching rate measurements versus temperature are shown in Figure 1a for peptide sequences (BODIPY-TMR)-$[Pro]_n$-Arg^+-Trp (n = 4 and 10, referred to herein as Pro_4 and Pro_{10}), (BODIPY-TMR)-$(Pro)_4$-Arg^+ (referred to as Pro_4 sans Trp), and (BODIPY-TMR)-$[Pro]_4$-Arg^+-Trp without the dye linker (referred to as Pro_4 sans X). Detailed discussion of the results for each peptide sequence is presented in reference [1].

Assuming the fluorescence is emitted by a population decaying from a single excited electronic state, the lifetime, τ, is given by $1/\tau = 1/\tau_0 + k_q$, where τ_0 is the unperturbed lifetime and k_q is the quenching rate constant representing a non-radiative decay process. The quenching rates shown in Figure 1a were calculated using a value for τ_0 obtained by fitting the expression $\tau = \tau_0/(1 + \tau_0 k_q)$ to the lifetime versus temperature measurements. It is important to point out that fragmentation was not observed in any of the fluorescence lifetime measurements as a result of the low average laser power (15 mW) and short exposure time used to measure decay times.

Figure 1a exhibits fits of the quenching rate to a phenomenological model, which relates the temperature dependence to spatial fluctuations of the peptide

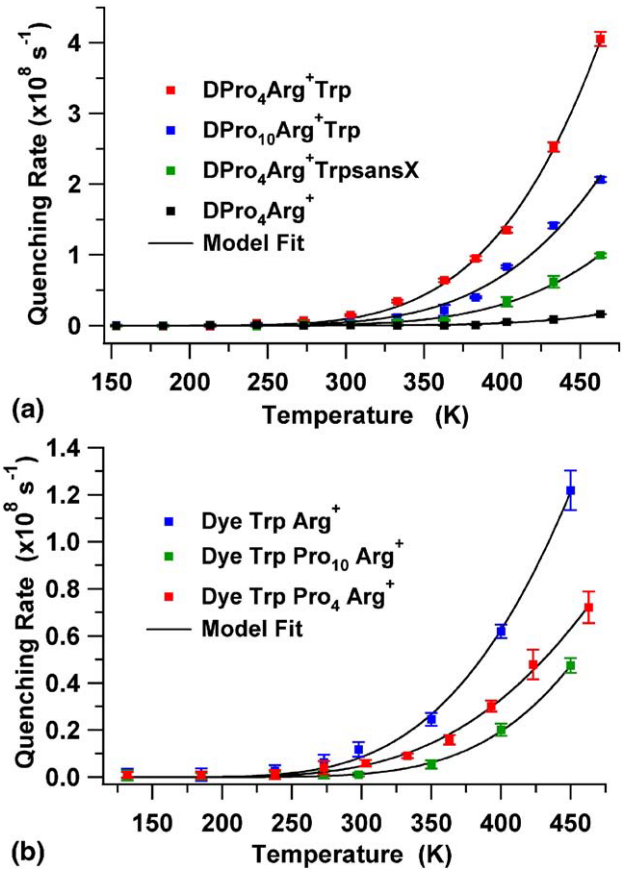

Figure 1. Quenching rates versus temperature for the $[M + H]^+$ polyproline ions (**a**) comparing variants of the sequence dye-$[Pro]_n$-Arg^+-Trp, and (**b**) comparing variants of dye-Trp-$[Pro]_n$-Arg^+. Individual curves are identified by the legends and the quenching rate fit to eq 1 is shown by solid lines. Error bars indicate the $\pm\sigma$ values from three replicate measurements performed for each data point.

conformation. This model describes the quenching rate, k_q, as a first-order Arrhenius process

$$k_q = k_f = A_f \exp(-E_{bf}/kT) \quad (1)$$

where k_f is the rate of fluctuations, which form conformers that quench the fluorescence. In eq 1, A_f represents an ensemble averaged rate characterizing those fluctuations and A_f is expected to represent collective side-chain fluctuations having rates $\sim 10^{11}-10^{12}$ s^{-1} or slower backbone motions $\sim 10^{10}$ s^{-1}. The spatial fluctuations leading to quenching conformers are constrained by energy barriers described by E_{bf}. The temperature T is the thermal equilibrium temperature established for the trapped peptide ions by He collisions and radiative interactions. The quenching rate model fits the lifetime data very closely for each peptide species in Figure 1a for the fit parameters listed in Table 1. These fit parameters will not be discussed further here except to point out that the prefactors $A_f \sim 10^{11}$ s^{-1} suggest the importance of side-chain fluctuations; and that values for E_{bf} are comparable to charge–dipole interaction energies between the dye and protonation site.

Fluorescence Quenching Rates for Dye-Trp-$[Pro]_n$-Arg^+

Fluorescence-quenching rate measurements versus temperature are shown in Figure 1b for peptide sequences (BODIPY-TMR)-Trp-$[Pro]_n$-Arg^+ ($n = 4$ and 10, referred to herein as DW Pro_4 and DW Pro_{10}), (BODIPY-TMR)-Trp-Arg^+ (referred to as DW). The lifetime measurements for these peptides demonstrate that electrostatic interactions introduced by the Arg protonation site strongly influence the quenching rates. In these peptide sequences, the dye and Trp residue are adjacent to one another and the absence of the dye linker ensures dye-Trp proximity for a larger fraction of the time. However, as shown in Figure 1b, the quenching rates for DW Pro_4 are comparable to Pro_4 sans X (Figure 1a), suggesting that additional factors play a significant role in the quenching mechanism. The quenching rates shown in Figure 1b for increasing polyproline chain lengths indicate a strong dependence on the average separation of the charged Arg side-chain and the dye-Trp pair. Fit parameters for these quenching rates using eq 1 are included in Table 1 and indicate that the prefactors $A_f \sim 10^{10}$ s^{-1} for these sequences are more characteristic of slower backbone fluctuations.

The polyproline peptide data provide evidence that the electrostatic fields of the protonation site play an important role in determining the quenching rate. It will be shown in the results of the MD simulations that electrostatic interactions introduced by the Arg protonation site can significantly change the exothermicity for an electron-transfer reaction between Trp and dye.

Molecular Dynamics Simulations for Dye-Trp-$[Pro]_4$-Arg^+

Molecular dynamics simulations of unsolvated $(M + H)^+$ ions of dye-Trp-$[Pro]_4$-Arg^+ were performed at seven temperatures over the range 200–500 K to study fluctuations of the dye, Trp, and Arg^+ relevant to the quenching interaction. These calculations have been useful to identify characteristics of conformers for which the quenching interaction is highly probable. These MD simulations are not expected to yield quantitative results which can be compared directly with experimentally measured quantities. Comparison with

Table 1. Polyproline fit parameters

Peptide	τ_0 (ns)[c]	A_f (10^{11} s^{-1})[c]	E_{bf} (eV)[c]
Pro_4	10.1 ± 0.1	4.1 ± 0.6	0.28 ± 0.01
Pro_4 sans X[a]	10.3 ± 0.1	2.1 ± 0.7	0.31 ± 0.01
Pro_{10}	11.1 ± 0.1	2.4 ± 0.9	0.28 ± 0.01
DW[b]	10.1 ± 0.1	0.24 ± 0.05	0.21 ± 0.01
$DWPro_4$[b]	10.6 ± 0.1	0.11 ± 0.02	0.20 ± 0.01
$DWPro_{10}$[b]	10.9 ± 0.4	0.59 ± 0.14	0.28 ± 0.01

[a]Sans X denotes the dye without linker.
[b]Structures for these peptides do not include dye linker.
[c]Uncertainties indicated are $\pm 1\sigma$.

gas-phase experiments in which unshielded charges give rise to strong electrostatic fields renders comparison with data especially sensitive to force field properties, including (1) parameterization of the electric charge and (2) the polarizability of the residues. As a consequence, the MD simulations for Pro_4 were performed to qualitatively describe the structures of quenching conformers to help identify a quenching mechanism that is consistent with the quenching rate data. One of the more useful results of the MD simulations for Pro_4 was to recognize that the electrostatic environment present in gas-phase biomolecules might be sufficient to induce fluorescence-quenching by charge-transfer between the dye and Trp residue assisted by the intramolecular electric fields.

Solution measurements performed in our laboratory [1] were able to unambiguously characterize the quenching interaction between the BODIPY TMR dye and Trp as photoinduced electron-transfer. A value of ΔE(dye-Trp) = −0.52 eV was estimated [1] for the exothermicity of a charge-transfer reaction between BODIPY-TMR and Trp, indicating that the quenching interaction is dominated by photoinduced electron-transfer in solution. However, an estimate for the exothermicity of electron-transfer in neutral, gas-phase Pro_4 yields ΔE(dye-Trp) = +1.6 eV, indicating a highly endothermic reaction.

The dye-Trp and dye-Arg^+ trajectories from MD simulations at 500 K are shown in Figure 2a and b, respectively. The exothermicity, ΔE, was estimated [1] for MD trajectories of $[M + H]^+$ ions by including Coulomb interaction energies of the charge on Arg^+ with the charge-separated pair Trp^+, and dye^- and with the dipole moments and the electronic polarizabilities of each residue. Figure 2c shows that fluctuations of the dye and Trp can result in quenching conformations for which charge-transfer becomes an exothermic reaction, $\Delta E < 0$, and *simultaneously* have dye-Trp separations ≤10Å. It should be noted, however, that the fluctuations of reaction exothermicity are very closely correlated with the dye-Arg^+ fluctuations, indicating that the exothermicity requires strong dye-Arg^+ interactions.

A description of the quenching process that emerged from the polyproline measurements was that the excited dye probes the ensemble of peptide conformations by spatial fluctuations until the occurrence of specific conformers which induce nonradiative decay. Experiments as well as the results of MD simulations suggest that these quenching conformers involve not only a reaction between the dye and Trp, but also require the presence of electrostatic fields from protonated side chains. The following sections describe fluorescence measurements of vancomycin noncovalent complexes and Trp-cage proteins. These were performed to investigate how the quenching rates in larger biomolecules are related to changes in gas-phase conformations induced by intermolecular and intramolecular interactions.

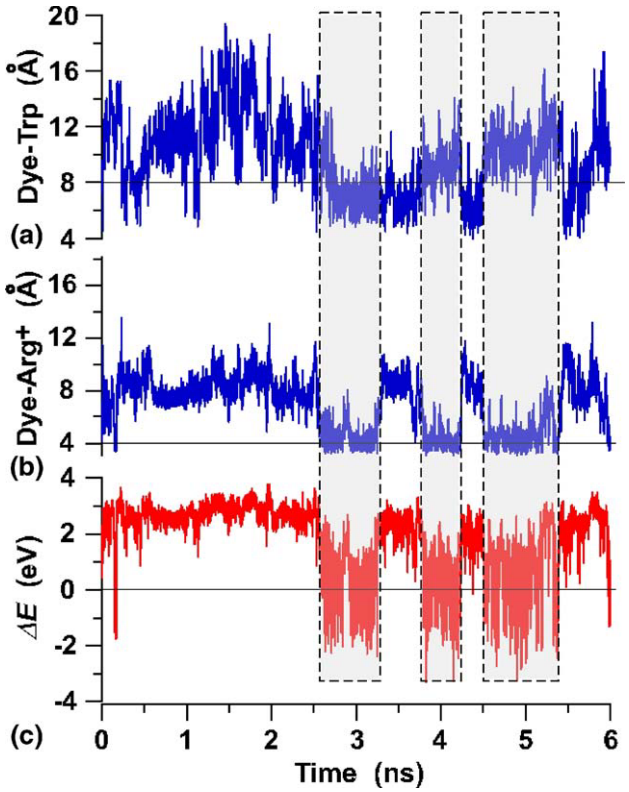

Figure 2. Trajectories of (**a**) the dye-Trp separation, and (**b**) the dye-Arg^+ separation from an MD simulation at 500 K for the sequence dye-$[Pro]_4$-Arg^+-Trp. Calculation of (**c**) the exothermicity fluctuations, ΔE, for a charge-transfer reaction using trajectories are described in the text. Vertical shaded regions bounded by the dashed lines are indicators for correlated fluctuations discussed in the text.

Vancomycin–Peptide Noncovalent Complexes

Vancomycin is an important therapeutic agent used for the treatment of gram-positive bacterial infections. Inhibition of bacterial cell-wall growth by vancomycin is based on noncovalent binding of the antibiotic to cell-wall precursors containing the C-terminal sequence KAA (LDD) [15–17]. The solution-phase structures of complexes formed between the vancomycin-group antibiotics and several small bacterial cell-wall mimicking peptides have been elucidated using NMR spectroscopy [3, 18–20] and X-Ray [6, 21, 22]. Electrospray ionization mass spectrometry (ESI-MS) has been applied to study vancomycin–peptide complexes in gas phase [23–32]. These gas-phase ESI-MS studies have determined the stoichiometry of vancomycin complexes and relative binding affinities for D/L-peptide stereoisomers.

The extensive research on vancomycin–peptide complexes suggest they are ideal systems to use for studies of noncovalent interactions with fluorescence techniques. The intermolecular interactions between dye-derivatized vancomycin (VD) and different peptide ligand stereoisomers can result in different conformations derived from different hydrogen binding configurations. Can such differences in conformation be cor-

related with quenching rate versus temperature curves? To consider this possibility, the fluorescence lifetime versus temperature was measured for complexes formed by VD with peptide ligands including a Trp residue as shown in Figure 3.

Since the disaccharide group shown in Figure 3 is not essential for the ligand recognition [33], derivatization of the dye on the primary amine of vancosamine is not expected to interfere with the complex hydrogen bond network. Based on our previous work on polyproline peptide dynamics in gas phase [1], BODIPY-R6G was coupled to vancosamine without a flexible linker to more closely reflect the conformational changes of the noncovalent complexes. This dye placement site identifies the charge site with certainty on the secondary amino group indicated in Figure 3. To ensure that dye interference in complex formation is minimal, vancomycin and VD at equimolar concentrations were mixed with peptide KAA (LDD) in solution and ESI-MS was performed. The full scan ESI-MS spectra in positive mode indicates that ion abundances for singly charged complexes formed with VD and vancomycin are similar (data not shown), supporting the assumption that dye attachment does not significantly interfere with the formation of the noncovalent complex. Singly charged cations thus provided a well defined model complex, which made interpretation of the fluorescence lifetime analysis more straightforward.

Time-resolved measurements of the fluorescence decays were performed on $[VD + H]^+$ and complexes of

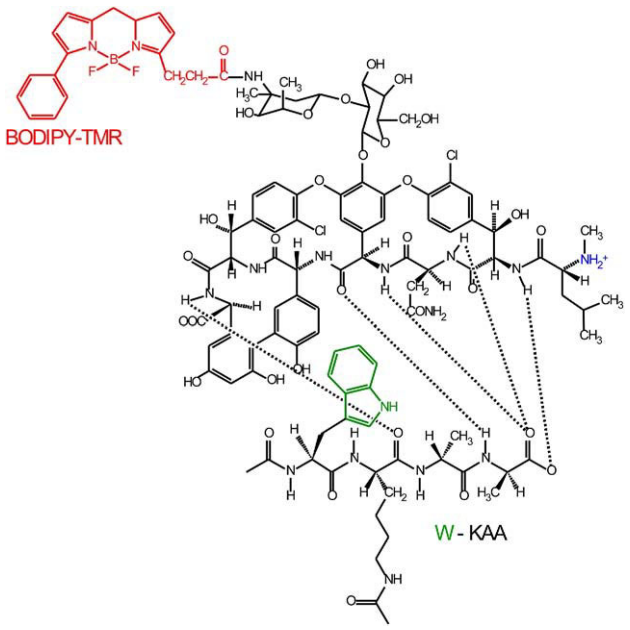

Figure 3. Noncovalent complex formed between dye-derivatized vancomycin and the tetrapeptide Ac2-L-Trp–L-Lys-D-Ala-D-Ala. The dye structure and binding on vancomycin is indicated in red and the Trp side-chain and binding site on the peptide is indicated in green. The secondary amine protonation site is indicated in blue. Dotted lines indicate hydrogen bonds identified in NMR solution studies of the vancomycin–KAA complex.

Table 2. The peptides used to form vancomycin complexes

	Sequence[a]	Abbreviation
1	L-Lys-D-Ala-D-Ala	KAA (LDD)
2	D-Lys-L-Ala-L-Ala	KAA (DLL)
3	D-Trp-L-Lys-D-Ala-D-Ala	W-KAA (D-LDD)
4	L-Trp-L-Lys-D-Ala-D-Ala	W-KAA (L-LDD)
5	L-Trp-D-Lys-L-Ala-L-Ala	W-KAA (L-DLL)

[a]Acetylation of the N-terminus and side chain amine of Lys.

VD with the peptides listed in Table 2 as a function of temperature over the range 153 to 398 K. As a control for the quenching measurements, fluorescence lifetimes were measured in the absence of Trp as a function of temperature from 189 to 398 K for $[VD + H]^+$ and the complex $[VD + KAA(LDD) + H]^+$. The fluorescent lifetimes in the absence of Trp are constant for temperatures less than ~350 K and decrease by ≤8% between 350 and 400 K (data not shown). This residual quenching is most probably the result of weak interactions with the remaining vancomycin residues or related to the dye photophysics at higher temperatures.

The measurements and preliminary MD simulations [34] for the three complexes with stereoisomer peptides W-KAA (D-LDD), (L-LDD), and (L-DLL) will be presented below. The discussion will concentrate on comparing results for (a) (D-LDD) and (L-LDD), and (b) (L-LDD) and (L-DLL). This will emphasize the most important characteristics of the data and their implications leaving details derived from a more complete analysis to be presented elsewhere.

Comparison of W-KAA (D-LDD) and (L-LDD) Complexes

The dependence of the quenching rates on the chirality of Trp is an important issue. Since the orientation of the Trp ring structures relative to the peptide backbone are significantly different for D and L chiralities, it was helpful to determine to what extent steric effects changed the quenching rate.

Results of quenching rate measurements for $[VD + W\text{-}KAA (D\text{-}LDD) + H]^+$ and $[VD + W\text{-}KAA (L\text{-}LDD) + H]^+$ ions are displayed in Figure 4a. The quenching rate is clearly sensitive to the change in chirality of a single Trp residue. This is most likely due to the steric effects of the Trp orientation modifying the hydrogen binding and, as a result, the conformation. The difference in the quenching rate fits is primarily the lower E_{bf} barrier parameter for (L-LDD) (Table 3). These quenching rates are comparable to those observed for the dye-Trp-$[Pro_n]$-Arg^+ with n = 4,10 suggesting that these rates are probably limited by the electrostatic fields.

MD structures calculated for stereoisomer complexes with different Trp chiralities are shown in Figure 5a and b and Figure 6 a and b. The structures for $[VD + W\text{-}KAA (L\text{-}LDD) + H]^+$ and $[VD + W\text{-}KAA (D\text{-}LDD) + H]^+$ ions are shown in Figure 5a and b, respectively. Figure 5a

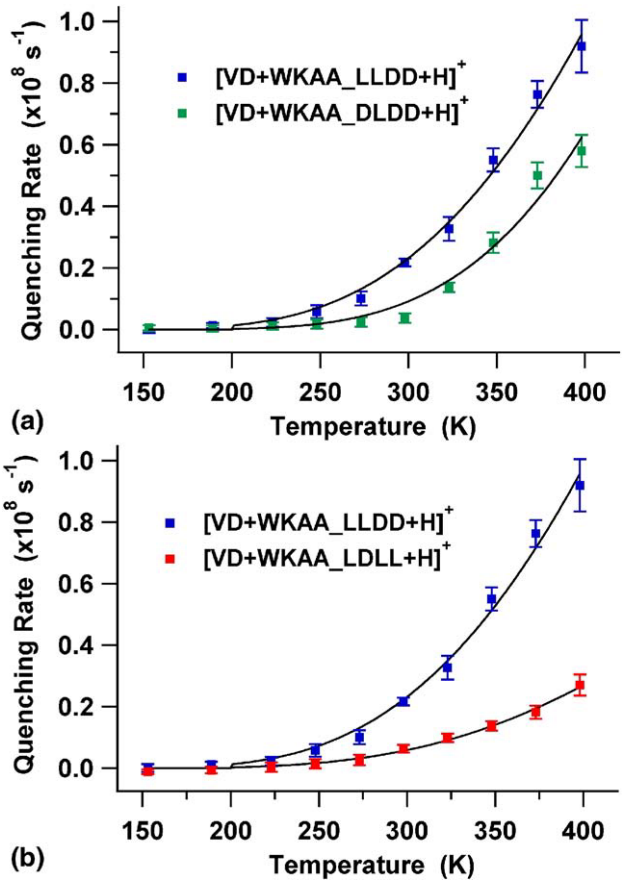

Figure 4. Quenching rates versus temperature for $[VD + H]^+$ complexes (**a**) comparing W-KAA (L-LDD) and W-KAA (D-LDD) peptides, and (**b**) comparing W-KAA (L-LDD) and W-KAA (L-DLL) peptides. Three replicate fluorescence decay time measurements are performed for each data point. Individual curves are identified by the legends and the quenching rate fit to eq 1 is shown by solid lines. Error bars indicate the $\pm\sigma$ values from three replicate measurements performed for each data point.

indicates that the bond between the disaccharide ligand and vancomycin allows sufficient flexibility for the dye fluctuations to probe the complex. The relative position of vancomycin and peptide are similar for both (D-LDD) and (L-LDD) complexes. The different orientations of the D/L Trp rings are clearly visible and the Trp orientation for (D-LDD) toward the body of vancomycin could be interfering with hydrogen bonding. These considerations are consistent with the structures shown in Figure 6a and b. Overlays of two structures that were taken at an arbitrary time (0.8 ns) for two different starting structures at 450 K are shown for the (L-LDD) complex in Figure 6a and for (D-LDD) in Figure 6b. To emphasize the vancomycin structures, the dye and peptide have been removed from the structure images. Clearly the structure for (L-LDD) suggests a more rigid structure than for (D-LDD) and the important question to be considered in the more complete analysis is whether this flexibility is directly related to the hydrogen bonds, and also how these structures vary with temperature.

Comparison of W-KAA (L-LDD) and (L-DLL) Complexes

The temperature dependence of the quenching rate for $[VD + W\text{-}KAA\ (L\text{-}DLL) + H]^+$ ions is dramatically different from $[VD + W\text{-}KAA\ (L\text{-}LDD) + H]^+$ ions as shown in Figure 4b. The maximum quenching rate of the L-LDD complex is a factor of ~3 greater than that of the L-DLL complex at 398 K. The model fits yield similar energy barriers, E_{bf}, but the fluctuation rate leading to quenching conformers, A_f, for L-LDD is greater than L-DLL by a factor of ~3.

The MD structures calculated for $[VD + W\text{-}KAA\ (L\text{-}LDD) + H]^+$ and $[VD + W\text{-}KAA\ (L\text{-}DLL) + H]^+$ ions are shown in Figure 5a and c, respectively. These structures indicate that the peptide positions are different for these complexes. Perhaps more significant, the overlays for different starting structures in Figure 6 show that the (L-DLL) complex is the most flexible of all the complexes at 450 K. These comparisons are currently being performed as a function of temperature for starting structures.

The trends of the dye-charge trajectory shown in Figure 7 show the dye-charge separations at 450 K are at the largest separations (14–18 Å) for the (L-DLL) complex and at shortest separation (3.5–7 Å) for the (L-LDD) complex consistent with the quenching rate magnitudes measured at 450 K. Although greater flexibility in the (L-DLL) complex allows side-chain fluctuations to sample a larger spatial range, apparently this does not insure a larger fraction of quenching conformations will be sampled. In fact, the MD trajectories indicate that the compactness of the more rigid (L-LDD) complex has the advantage to sample a greater fraction of quenching conformers. These quenching rate measurements imply that the probability of forming quenching conformers by spatial fluctuations is very sensitive to the peptide sequence chiralities and thus retain the characteristic of molecular recognition described in previous studies of these noncovalent complexes.

Table 3. Vancomycin complex fit parameters

Complex[a]	τ_0 (ns)[b]	A_f (s^{-1})[b]	E_{bf} (eV)[b]
$[VD + WKAA\ (L\text{-}DLL) + H]^+$	11.4 ± 0.4	2.5 ± 0.7 e+9	0.16 ± 0.01
$[VD + WKAA\ (D\text{-}LDD) + H]^+$	11.2 ± 0.1	2.2 ± 1.5 e+10	0.20 ± 0.02
$[VD + WKAA\ (L\text{-}LDD) + H]^+$	11.2 ± 0.1	7.3 ± 1.8 e+9	0.15 ± 0.01

[a]All structures do not include dye linker.
[b]Uncertainties indicated are $\pm 1\sigma$.

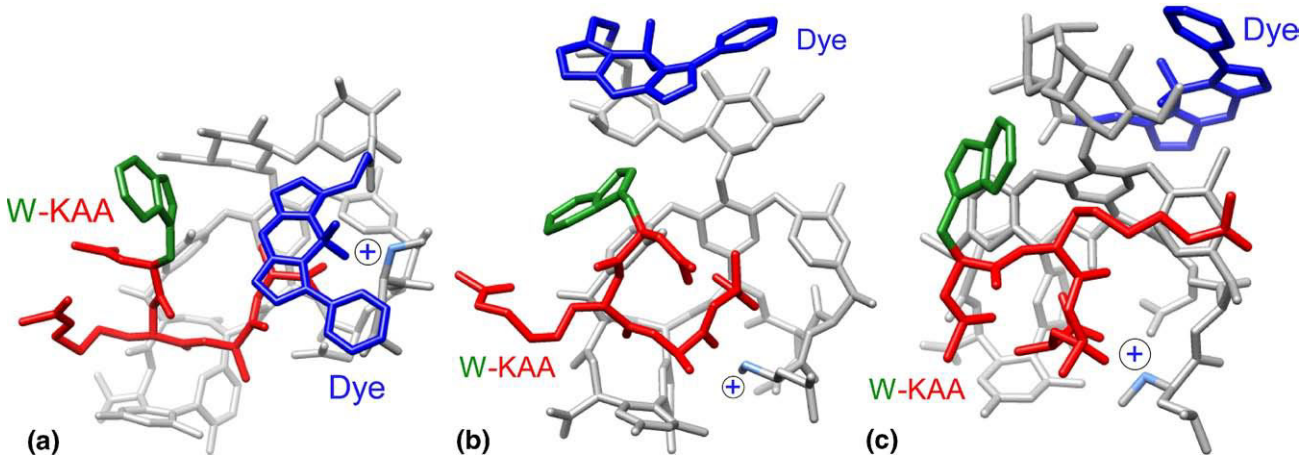

Figure 5. Representative structures of $[VD + WKAA + H]^+$ complexes calculated at 450 K for (**a**) W-KAA (L-LDD), (**b**) W-KAA (D-LDD), and (**c**) W-KAA (L-DLL). The Trp side chain, KAA peptide, and the dye are indicated in green, red, and blue, respectively, and vancomycin is indicated in grey. The protonation site in light blue is indicated by the encircled plus sign.

The dication complexes $[VM + KAA(DLL) + 2H]^{2+}$ and $[VM + KAA(LDD) + 2H]^{2+}$ have been studied in previous dissociation measurements [27] and exhibit identical binding energies. Although these quenching measurements cannot draw a conclusion regarding the relative binding energy of these monocation complexes of L-DLL and L-LDD, they indicate remarkable differences in the dynamic properties. A detailed gas-phase study [35] of the $[VM + KAA(LDD) + H]^+$ monocation by surface-induced dissociation and related DFT calculations identifies roughly similar placement for the peptide binding as suggested by the MD structure in Figure 5a and b. Furthermore, results for the vancomycin–KAA complex indicate a gas-phase structure significantly different from the solution phase structure [35].

Trp-Cage Protein

Trp-cage is a 20-residue miniprotein, which has been shown to be fully structured in aqueous solution at low temperatures [4]. The folded structure has a compact hydrophobic core consisting of a Trp side chain that is "caged" by several hydrophobic residues. The NMR structure of the Trp-cage also indicates a salt bridge between the negatively charged aspartic acid (Asp) at position 9 and the positively charged lysine (Lys) and arginine (Arg) at positions 8 and 16, respectively [4]. Trp-cage is remarkable in that it is the smallest example of a protein with cooperatively folded tertiary structure in aqueous solution [4, 36], and that it folds in only 4 μs [37]. Miniproteins such as Trp-cage are useful tools for

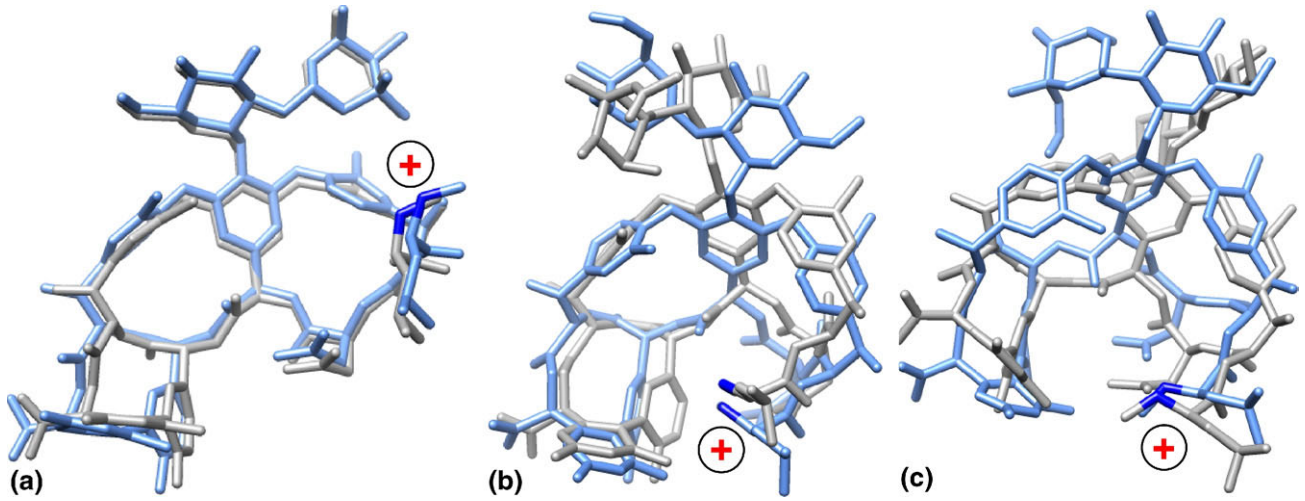

Figure 6. Representative structures of $[VD + WKAA + H]^+$ complexes calculated at 450 K from two starting structures for (**a**) W-KAA (L-LDD), (**b**) W-KAA (D-LDD), and (**c**) W-KAA (L-DLL). The dye and peptide have been deleted from the image to emphasize the vancomycin structures indicated by light blue and grey. The protonation site in dark blue is indicated by the encircled plus sign.

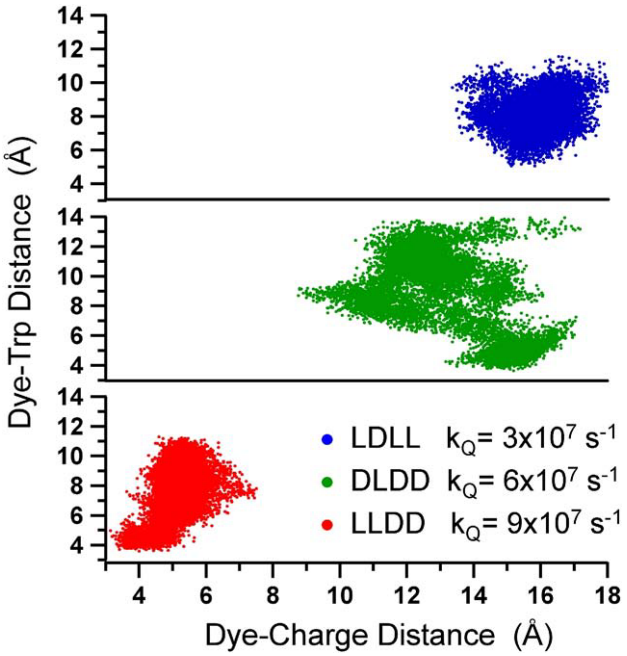

Figure 7. Dye-Trp distance versus dye-charge distance from trajectories calculated at 450 K for $[VD + WKAA + H]^+$ complexes with W-KAA (L-DLL), W-KAA (D-LDD) and W-KAA (L-LDD). Individual peptide plots are identified by the legend which also indicates the quenching rate measured at 450 K. Each point represents the distances after an MD interval of 0.1 ps.

the study of protein folding because their small size makes them amenable to chemical synthesis which expedites the production of variants for mutational studies [4, 36]. In addition, they are readily tractable by molecular dynamics simulations [38–44].

Here, we present fluorescence lifetime measurements of Trp-cage as a function of temperature in gas phase, examining the role of charge state. The present study concentrates on applying fluorescence-quenching rates to determine the importance of a salt bridge in stabilizing the structure in gas phase. It has been established that the salt bridge is essential for stability of the folded protein [4] in solution phase. In view of that, measurements were performed for two amino acid sequences discussed in the Materials section.

Wild Trp-cage: NLYIQWLK***D***GGPSSGRPPPSK-(BODIPY-TMR)-$CONH_2$

D9N Trp-cage: NLYIQWLK***N***GGPSSGRPPPSK-(BODIPY-TMR)-$CONH_2$.

The only difference in these sequences is the single point mutation in D9N Trp-cage in which aspartic acid (Asp9) has been replaced by asparagine (Asn), which eliminates the possibility that the + − + salt bridge can form in gas phase between Lys8, Asp9, and Arg16 as it does in solution [4]. MD simulations are being performed as a function of charge state, salt bridge, and temperature to elucidate details of the dye-protein conformational dynamics leading to the observed changes in fluorescence-quenching rates. Several of the preliminary structures will be presented to correlate with the measured quenching rates.

Figure 8 presents the quenching rates versus temperature data obtained over the range 150–453 K. The wild Trp-cage data for the 3+, 2+, and 1+ charge states are shown in Figure 8a. These data exhibit similar curves for the 3+ and 2+ states but significantly higher quenching rates for the 1+ state. Table 4 lists the quenching model fit parameters for these charge states which reflect these trends. Earlier fluorescence intensity measurements [9, 45] indicated that the intensity versus

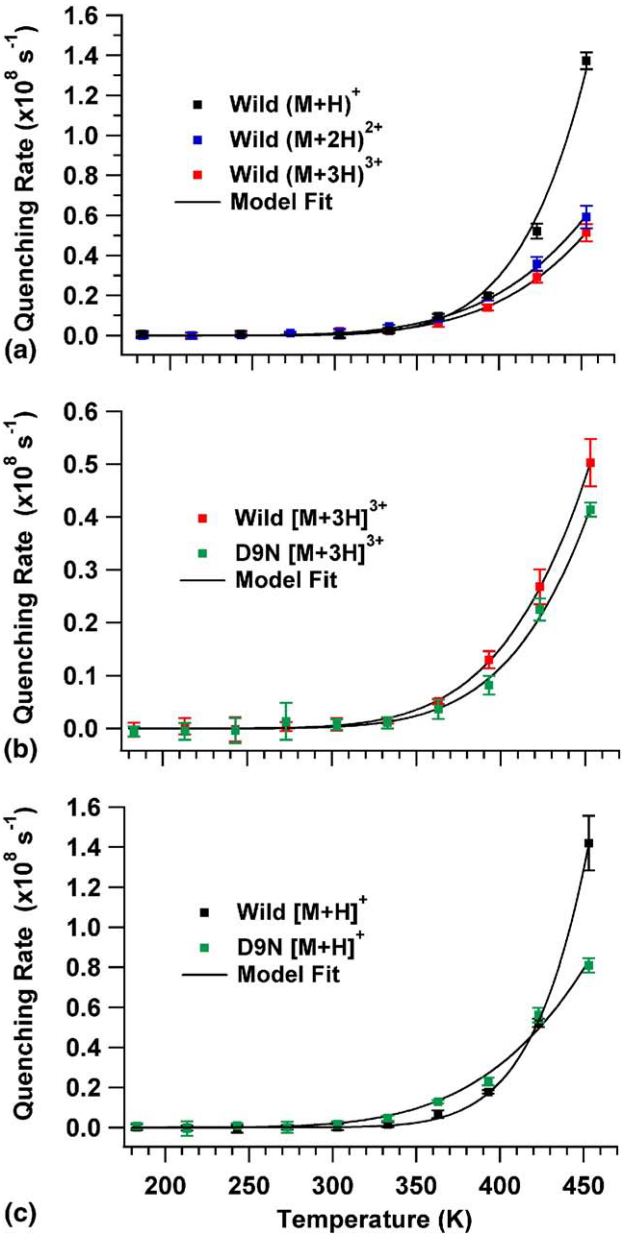

Figure 8. Quenching rates versus temperature for Trp-cage ions (**a**) comparing 1+, 2+, and 3+ charge states for the wild Trp-cage sequence, (**b**) comparing wild Trp-cage and D9N Trp-cage sequences for $[M + 3H]^{3+}$ ions, (**c**) comparing wild Trp-cage and D9N Trp-cage sequences for $[M + H]^+$ ions. Individual curves are identified by the legends and the quenching rate fit to eq 1 is shown by solid lines. Error bars indicate the $\pm\sigma$ values from three replicate measurements performed for each data point.

Table 4. Trp-cage fit parameters

Protein[a]	τ_0 (ns)[b]	A_f (s^{-1})[b]	E_{bf} (eV)[b]
Wild $[M + 3H]^{3+}$	10.9 ± 0.02	2.1 ± 0.5 e+11	0.32 ± 0.01
Wild $[M + 2H]^{2+}$	10.9 ± 0.03	1.5 ± 0.2 e+11	0.31 ± 0.01
Wild $[M + H]^{+}$	11.30 ± 0.03	1.1 ± 0.1 e+13	0.44 ± 0.01
D9N $[M + 3H]^{3+}$	11.19 ± 0.05	4.7 ± 3.3 e+11	0.47 ± 0.03
D9N $[M + H]^{+}$	11.30 ± 0.11	2.4 ± 1.7 e+11	0.31 ± 0.01

[a]All structures include dye linker.
[b]Uncertainties indicated are $\pm 1\sigma$.

temperature in the presence of fluorescence-quenching exhibited a decrease of intensity for the 2+ state, which was significantly less than for the 3+ charge state. In a paper discussing fluorescence intensity measurements in polyproline peptides [46], it was estimated that intramolecular electrostatic fields were sufficiently strong ($\sim 10^7 - 10^8$ V/cm) to shift the dye emission spectrum by ~20 nm. The intensity reduction in such fields would lead to spectral shifts outside the bandwidth of filters in the collection optics and thus would be present even in the absence of Trp as was observed for polyproline peptides [46]. Consequently, the intensity measurements of Trp-cage in each charge state was probably a combination of fluorescence-quenching and filter loss that would be strongly dependent on charge state. In this regard, lifetime quenching is an intrinsic process that avoids effects derived from intensity variation. It is interesting to point out that the MD simulations complementing the intensity measurements [9] indicated that the Trp-cage structures in gas phase were comparably compact in both 2+ and 3+ charge states, consistent with the present quenching rate measurements.

Comparisons of quenching rate versus temperature for wild Trp-cage and D9N Trp-cage sequences are displayed in Figure 8b and c for the 3+ and 1+ charge states, respectively. In the 3+ state shown in Figure 8b, the quenching rate curves for both sequences are very similar in both magnitude and shape indicating that the structure of this charge state does not include a salt bridge. A similar result was observed for the 2+ charge state (data not shown). Thus the salt bridge, though an important contributor to stability in solution, does not appear to be a significant contributor to the observed stability of these gas-phase ions. However, quenching rate curves for these sequences shown in Figure 8c for the 1+ state display a significant difference both in magnitude and shape. The fit parameters in Table 4 indicate similar values for all species and charge states except the wild Trp-cage sequence for 1+, suggesting that a salt bridge plays a role in only this species. These results are particularly interesting in light of ultraviolet photodissociation measurements [47] of Trp-cage in the 1+ charge state, which infer the presence of a salt bridge structure and MD calculations [48] on the 1+ state that characterize the Trp-cage structure with a salt bridge present.

MD simulations are currently being performed [49] over the experimental temperature range to relate the quenching rate measurements to the charge state structures. Preliminary structures for the 1+ charge state are shown in Figure 9. The D9N Trp-cage structure in Figure 9a is qualitatively similar to compact structures calculated [9] previously for the 2+ and 3+ states. The MD simulation for the wild Trp-cage structure (Figure 9b) was performed with charges placed on $Lys8^+$, $Asp9^-$, and $Arg16^+$ to form a + − + salt bridge. The salt bridge will constrain the spatial fluctuations of these charge sites possibly resulting in stronger electro-

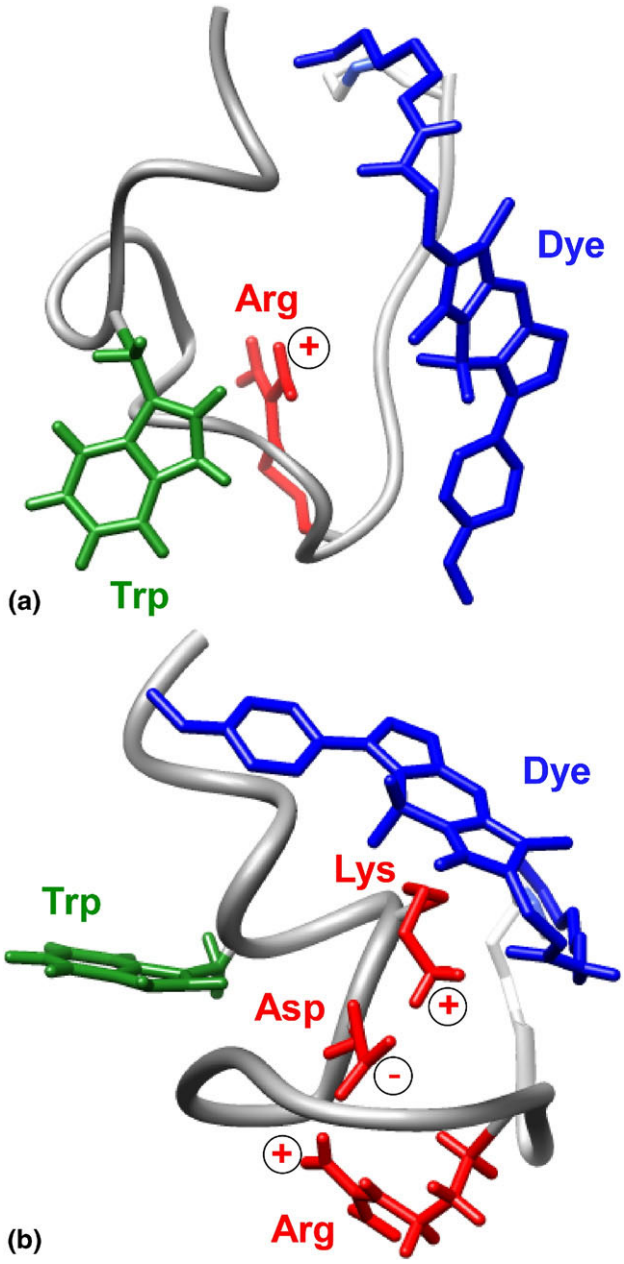

Figure 9. Representative structures of Trp-cage $[M + H]^+$ ions calculated at 315 K for (**a**) D9N Trp-cage sequence, and (**b**) wild Trp-cage sequence. In D9N Trp-cage the Trp residue is in green, Arg residue in red, dye in blue, and Trp-cage backbone in grey. The protonation site on Arg is indicated by the encircled plus sign. In the wild Trp-cage sequence a salt bridge structure indicated by (+ − +) is shown between Lys, Asp, and Arg residues in red.

static interactions with the fluctuating dye. In contrast, the D9N Trp-cage charge site on the Arg side chain is free to fluctuate over a larger spatial range increasing the average dye-charge separation, which has been noted above in the polyproline peptide to result in lower quenching rates. Additionally, the salt bridge appears to constrain the separation between the dye and Trp side chain, which will also tend to increase the quenching rate. In continuing analysis, the structures for each charge state will be considered as a function of temperature to identify the dependence of quenching rate on structure more quantitatively.

Conclusions

Quenching rate measurements of polyproline peptide sequences provided an opportunity to control the intramolecular interactions so that the characteristics of conformers, which had a high probability to quench the fluorescence, could be determined. Quenching was increased by the presence of a strong electrostatic field in the vicinity of the fluorescent dye and in addition by the proximity of the dye and Trp side chain. The spatial constraints imposed by these requirements imply that those quenching conformers satisfying these constraints are probably a small subset of the total ensemble of fluctuating conformations. A model for the quenching mechanism based on field enhanced electron-transfer between the Trp and dye is consistent with the experimental quenching data.

Quenching data for larger biomolecular structures display distinct changes in the rate versus temperature curves driven by intramolecular interactions in Trp-cage protein and intermolecular interactions in vancomycin–peptide complexes. The presence of a salt bridge structure in the Trp-cage protein was shown to be strongly dependent on charge state. The salt bridge is inferred from the quenching rate of the 1+ charge state by comparing rates of the wild type with a mutant in which the salt bridge is eliminated by a variant amino acid sequence. The increased quenching rate observed when the salt bridge is present is most likely associated with more compact conformations. As indicated by MD simulations, these conformations decrease the dye-Trp and dye-Arg^+ separations, which lead to increased quenching rates based on the quenching model. The continuing analysis of MD trajectories is quantifying these results as a function of starting structure and temperature. The quenching rate in vancomycin–peptide complexes was observed to be dependent on the chirality of the peptide amino acids. The quenching rate was shown to be sensitive to a change in chirality of a single Trp residue in the peptide. Larger differences in quenching rates were observed for peptide chiralities, which were previously [27] associated with changes in the hydrogen bonding network. MD trajectories for different peptide chiralities indicate that decreases in the dye-Arg^+ separations are correlated with the measured increases in the quenching rates. These MD analyses are being extended to all temperatures and starting structures to obtain a more quantitative description of the dependence of peptide chirality on vancomycin flexibility and hydrogen bond probability.

Acknowledgments

The authors thank Professor David van der Spoel (Uppsala University) for preliminary MD calculations on Trp-cage and Drs. Zhibo Yang, Erich R. Vorpagel, and Julia Laskin (Pacific Northwest National Laboratory) for calculations performed on the vancomycin–peptide complexes. They also thank Dr. Albert J. R. Heck (Utrecht University) and Thomas J. D. Jørgensen (University of Southern Denmark) for helpful discussions. They recognize and thank Dr. Anthony Iavarone for suggesting the vancomycin study and for helpful discussions. Financial support by the National Science Foundation (Grant CHE-0962680) and The Rowland Institute at Harvard is gratefully acknowledged.

References

1. Shi, X.; Duft, D.; Parks, J. H. Fluorescence Quenching Induced by Conformational Fluctuations in Unsolvated Polypeptides. *J. Phys. Chem. B* **2008,** *112*, 12801–12815.
2. Molecular Probes. http://probes.invitrogen.com (accessed 10/2009).
3. Williams, D. H.; Williamson, M. P.; Butcher, D. W.; Hammond, S. J. Detailed Binding Sites of the Antibiotics Vancomycin and Ristocetin A: Determination of Intermolecular Distances in Antibiotic/Substrate Complexes by Use of the Time-Dependent NOE. *J. Am. Chem. Soc.* **1983,** *105*, 1332–1339.
4. Neidigh, J. W.; Fesinmeyer, R. M.; Andersen, N. H. Designing a 20-Residue Protein. *Nat. Struct. Biol.* **2002,** *9*, 425–430.
5. Iavarone, A. T.; Duft, D.; Parks, J. H. Shedding Light on Biomolecule Conformational Dynamics Using Fluorescence Measurements of Trapped Ions. *J. Phys. Chem. A* **2006,** *110*, 12714–12727.
6. (a) http://www.rcsb.org, and PDB code is 1aa5; (b) Loll, P. J.; Bevivino, A. E.; Korty, B. D.; Axelen, P. H. Simultaneous Recognition of a Carboxylate-Containing Ligand and an Intramolecular Surrogate Ligand in the Crystal Structure of an Asymmetric Vancomycin Dimer. *J. Am. Chem. Soc.* **1997,** *119*, 1516–1522.
7. Maple, J.; Dinur, U.; Hagler, A. T. Derivation of Force Fields for Molecular Mechanics and Dynamics from Ab Initio Energy Surfaces. *Proc. Natl. Acad. Sci. U.S.A.* **1988,** *85*, 5350–5354.
8. Tsallis, C.; Stariolo, D. A. Generalized Simulated Annealing. *Physica A* **1996,** *233*, 395–406.
9. Iavarone, A. T.; Patriksson, A.; Van der Spoel, D.; Parks, J. H. Fluorescence Probe of Trp-Cage Protein Conformation in Solution and in Gas Phase. *J. Am. Chem. Soc.* **2007,** *129*, 6726–6735.
10. Lindahl, E.; Hess, B.; Van der Spoel, D. GROMACS. 3.0: A Package for Molecular Simulation and Trajectory Analysis. *J. Mol. Mod.* **2001,** *7*, 306–317.
11. Van der Spoel, D.; Lindahl, E.; Hess, B.; Groenhof, G.; Mark, A. E.; Berendsen, H. J. C. GROMACS: Fast, Flexible, and Free. *J. Comp. Chem.* **2005,** *26*, 1701–1718.
12. Jorgensen, W. L.; Maxwell, D. S.; Tirado-Rives, J. Development and Testing of the OPLS All-Atom Force Field on Conformational Energetics and Properties of Organic Liquids. *J. Am. Chem. Soc.* **1996,** *118*, 11225–11236.
13. Hukushima, K.; Nemoto, K. Exchange Monte Carlo Method and Application to Spin Glass Simulations. *J. Phys. Soc. Jpn.* **1996,** *65*, 1604–1608.
14. Counterman, A. E.; Clemmer, D. E. Anhydrous Polyproline Helices and Globules. *J. Phys. Chem. B* **2004,** *108*, 4885–4898.
15. Perkins, H. R. Specificity of Combination between Mucopeptide Precursors and Vancomycin or Ristocetin. *Biochem. J.* **1969,** *111*, 195–205.
16. Nieto, M.; Perkins, H. R. Modifications of the Acyl-D-Alanyl-D-Alanine Terminus Affecting Complex-Formation with Vancomycin. *Biochem. J.* **1971,** *123*, 789–803.
17. Perkins, H. R. Vancomycin and Related Antibiotics. *Pharmacol. Ther.* **1982,** *16*, 181–197.
18. Rajagopalan, J. S.; Harris, C. M.; Harris, T. M. The Role of Phenolic Groups in Vancomycin-Type Glycopeptide Antibiotics. *Bioorg. Chem.* **1995,** *23*, 54–71.
19. Williams, D. H.; Westwell, M. S. The Fight Against Antibiotic-Resistant Bacteria. *Chemtech* **1996,** *26*, 17–23.
20. Williams, D. H.; Kalman, J. R. Structural and Mode of Action Studies on the Antibiotic Vancomycin. Evidence from 270-MHz Proton Magnetic Resonance. *J. Am. Chem. Soc.* **1977,** *99*, 2768–2774.
21. Loll, P. J.; Miller, R.; Weeks, C. M.; Axelsen, P. H. A Ligand-Mediated Dimerization Mode for Vancomycin. *Chem. Biol.* **1998,** *5*, 293–298.

22. Kaplan, J.; Korty, B. D.; Axelsen, P. H.; Loll, P. J. The Role of Sugar Residues in Molecular Recognition by Vancomycin. *J. Med. Chem.* **2001,** *44*, 1837–1840.
23. Hamdan, M.; Curcuruto, O.; Di Modugno, E. Investigation of Complexes between Some Glycopeptide Antibiotics and Bacterial Cell-Wall Analogues by Electrospray- and Capillary Zone Electrophoresis/Electrospray-Mass Spectrometry. *Rapid Commun. Mass Spectrom.* **1995,** *9*, 883–887.
24. Lim, H. K.; Hsieh, Y. L.; Ganem, B.; Henion, J. Recognition of Cell-Wall Peptide Ligands by Vancomycin Group Antibiotics—Studies Using Ion-Spray Mass-Spectrometry. *J. Mass Spectrom.* **1995,** *30*, 708–714.
25. Vollmerhaus, P. J.; Breukink, E.; Heck, A. J. R. Getting Closer to the Real Bacterial Cell Wall Target: Biomolecular Interactions of Water-Soluble Lipid II with Glycopeptide Antibiotics. *Chemistry* **2003,** *9*, 1556–1565.
26. Heck, A. J. R.; Bonnici, P. J.; Breukink, E.; Morris, D.; Wills, M. Modification and Inhibition of Vancomycin Group Antibiotics by Formaldehyde and Acetaldehyde. *Chemistry* **2001,** *7*, 910–916.
27. Jorgensen, T. J. D.; Delforge, D.; Remacle, J.; Bojesen, G.; Roepstorff. P. Collision-Induced Dissociation of Noncovalent Complexes Between Vancomycin Antibiotics and Peptide Ligand Stereoisomers: Evidence for Molecular Recognition in the Gas Phase. *Int. J. Mass Spectrom.* **1999,** *188*, 63–85.
28. Haselmann, K. F.; Jørgensen, T. J. D.; Budnik, B. A.; Jensen, F.; Zubarev, R. A. Electron Capture Dissociation of Weakly Bound Polypeptide Polycationic Complexes. *Rapid Commun. Mass Spectrom.* **2002,** *16*, 2260–2265.
29. Jørgensen, T. J. D.; Roepstorff, P. Direct Determination of Solution Binding Constants for Noncovalent Complexes between Bacterial Cell Wall Peptide Analogues and Vancomycin Group Antibiotics by Electrospray Ionization Mass Spectrometry. *Anal. Chem.* **1998,** *70*, 4427–4432.
30. Heck, A. J. R.; Jørgensen, T. J. D.; O'Sullivana, M.; Von Raumera, M.; Derrick, P. J. Gas-Phase Noncovalent Interactions between Vancomycin-Group Antibiotics and Bacterial Cell-Wall Precursor Peptides Probed by Hydrogen/Deuterium Exchange. *J. Am. Soc. Mass Spectrom.* **1998,** *9*, 1255–1266.
31. Jørgensen, T. J. D.; Hvelplund, P.; Andersen, J. U.; Roepstorff, P. Tandem Mass Spectrometry of Specific versus Nonspecific Noncovalent Complexes of Vancomycin Antibiotics and Peptide Ligands. *Int. J. Mass Spectrom.* **2002,** *219*, 659–670.
32. Heck, A. J. R.; Jorgensen, T. J. D. Vancomycin in Vacuo. *Int. J. Mass Spectrom.* **2004,** *236*, 11–23.
33. Gerhard, U.; Mackay, J. P.; Maplestone, R. A.; Williams, D. H. The Role of the Sugar and Chlorine Substituents in the Dimerization of Vancomycin Antibiotics. *J. Am. Chem. Soc.* **1993,** *115*, 232–237.
34. These MD simulations were performed by Zhibo Yang, Xiangguo Shi, Erich R. Vorpagel and Julia Laskin at the Pacific Northwest National Laboratory.
35. Yang, Z.; Vorpagel, E. R.; Laskin, J. Experimental and Theoretical Studies of the Structures and Interactions of Vancomycin Antibiotics with Cell Wall Analogues. *J. Am. Chem. Soc.* **2008,** *130*, 13013–13022.
36. Gellman, S. H.; Woolfson, D. N. Mini-Proteins Trp the Light Fantastic. *Nat. Struct. Biol.* **2002,** *9*, 408–410.
37. Qiu, L.; Pabit, S. A.; Roitberg, A. E.; Hagen, S. J. Smaller and Faster: The 20 Residue Trp-Cage Protein Folds in 4 μs. *J. Am. Chem. Soc.* **2002,** *124*, 12952–12953.
38. Simmerling, C.; Strockbine, B.; Roitberg, A. E. All-Atom Structure Prediction and Folding Simulations of a Stable Protein. *J. Am. Chem. Soc.* **2002,** *124*, 11258–11259.
39. Snow, C. D.; Zagrovic, B.; Pande, V. S. The Trp Cage: Folding Kinetics and Unfolded State Topology Via Molecular Dynamics Simulations. *J. Am. Chem. Soc.* **2002,** *124*, 14548–14549.
40. Pitera, J. W.; Swope, W. Understanding Folding and Design: Replica-Exchange Simulations of "Trp-cage" Miniproteins. *Proc. Natl. Acad. Sci. U.S.A.* **2003,** *100*, 7587–7592.
41. Chowdhury, S.; Lee, M. C.; Xiong, G. M.; Duan, Y. Ab Initio Folding Simulation of the Trp-Cage Mini-Protein Approaches NMR Resolution. *J. Mol. Biol.* **2003,** *327*, 711–717.
42. Zhou, R. Trp-cage: Folding Free Energy Landscape in Explicit Water. *Proc. Natl. Acad. Sci. U.S.A.* **2003,** *100*, 13280–13285.
43. Seshasayee, A. S. High-Temperature Unfolding of a Trp-Cage Mini-Protein: A Molecular Dynamics Simulation Study. *Theor. Biol. Med. Model.* **2005,** *2*, 7.
44. Ding, F.; Buldyrev, S. V.; Dokholyan, N. V. Folding Trp-Cage to NMR Resolution Native Structure Using a Coarse-Grained Protein Model. *Biophys. J.* **2005,** *88*, 147–155.
45. Iavarone, A. T.; Parks, J. H. Conformational Change in Unsolvated Trp-Cage Protein Probed by Fluorescence. *J. Am. Chem. Soc.* **2005,** *127*, 8606–8607.
46. Iavarone, A. T.; Meinen, J.; Schulze, S.; Parks, J. H. Fluorescence Probe of Polypeptide Conformational Dynamics in Gas Phase and in Solution. *Int. J. Mass Spectrom.* **2006,** *253*, 172–180.
47. Kjeldsen, F.; Silivra, O. A.; Zubarev, R. A. Zwitterionic States in Gas-Phase Polypeptide Ions Revealed by 157-nm Ultra-Violet Photodissociation. *Chem. Eur. J.* **2006,** *12*, 7920–7928.
48. Patriksson, A.; Adams, C. M.; Kjeldsen, F.; Zubarev, R. A.; Van der Spoel, D. A Direct Comparison of Protein Structure in the Gas and Solution Phase: The Trp-Cage. *J. Phys. Chem. B* **2007,** *111*, 13147–13150.
49. These MD simulations are being performed by David Van der Spoel at Uppsala University.